Temperature-driven transient charge and heat currents in nanoscale conductors

F. G. Eich, M. Di Ventra, and G. Vignale

Temperature-driven transient charge and heat currents in nanoscale conductors

F. G. Eich,[1, *] M. Di Ventra,[2] and G. Vignale[1]

[1]*Department of Physics, University of Missouri-Columbia, Columbia, Missouri 65211*
[2]*University of California - San Diego, La Jolla, CA 92093*
(Dated: February 1, 2016)

We analyze the short-time behavior of the heat and charge currents through nanoscale conductors exposed to a temperature gradient. To this end we employ Luttinger's thermo-mechanical potential to simulate a sudden change of temperature at one end of the conductor. We find that the direction of the charge current through an impurity is initially opposite to the direction of the charge current in the steady-state limit. Furthermore we investigate the transient propagation of energy and particle density driven by a temperature variation through a conducting nanowire. Interestingly, we find that the velocity of the wavefronts of, both, the particle and the energy wave have the same constant value, insensitive to changes in the average electronic density. In the steady-state regime we find that, at low temperatures, the local temperature and potential, as measured by a floating probe lead, exhibit characteristic oscillations due to quantum interference, with a periodicity that corresponds to half the Fermi wavelength of the electrons.

I. INTRODUCTION

The description of the combined charge and energy transport at the nanoscale has received a great deal of attention in recent years.[1–3] Much of the motivation is supplied by the search for efficient thermoelectric devices, which would allow, for example, partial conversion of waste heat into usable energy. Experimentally, several procedures have been developed to measure local temperatures at the nanometer scale, e.g., scanning thermal microscopy[4–8] and transmission electron microscopy.[9] On the theoretical side various approaches have been used to formally justify the extrapolation of well-established concepts of equilibrium statistical mechanics, such as temperature and entropy, to nonequilibrium nanoscale systems.[10–15]

A very interesting theoretical tool for the study of thermoelectric transport phenomena is the space- and time-dependent thermo-mechanical potential $\psi(\boldsymbol{r}, t)$, which was first introduced by Luttinger[16] to formulate the response of electrons to temperature gradients as a Hamiltonian problem. Like the gravitational field, to which it is formally related, the thermo-mechanical potential is linearly coupled to the energy density, for which Luttinger chose one of several possible definitions – all equivalent in the long-wavelength limit.

In recent years, Luttinger's idea has found several interesting applications in the calculation of the linear thermoelectric response of macroscopic systems.[17–21] In a recent paper, we have shown that the thermo-mechanical potential offers a natural path to the inclusion of thermoelectric effects in a general-purpose time-dependent density-functional theory.[22] Furthermore, we have shown that, when certain dynamical many-body effects are neglected, the thermo-mechanical potential formalism reproduces the results of the well-known Landauer-Büttiker[23–25] multi-terminal formalism for thermal transport[26] (see also Refs. 27,28 for a de-

scription of the so-called partition-free approach to quantum transport and its relation to the Landauer-Büttiker formalism) and allows a natural definition of the local temperature in terms of a local probe that carries no currents.[15,26,29]

The study of Ref. 26 focused on the steady-state response to voltage and temperature gradients. In this paper we present the first application of Luttinger's thermo-mechanical potential approach to the computation of transient particle and energy or heat currents through nanoscale devices.

We consider two model devices. The first one is a single impurity (quantum dot) sandwiched between two thermal reservoirs at different temperatures. The second model is a conducting chain of atoms placed between the same two reservoirs. In both cases we study the time evolution of the electronic and energy densities and the associated currents following a sudden change in the temperature of the left reservoir. This idealized set up, can actually be approximately realized in experiments, when the current in one of the heater coils typically used to set the temperatures of the reservoirs is suddenly increased or decreased.[2] Of course, in experiments the rate at which the temperature changes in that reservoir is limited by the inelastic processes involved (phonon and radiative dissipation). Here, since we are only interested in the quality behavior, we consider an instantaneous switch-on of the perturbation.

In the case of a single impurity, we find that the particle current for short times after the switch-on flows opposite to the particle current in the long-time (steady-state) limit, usually addressed within the Landauer-Büttiker[23–25] or Meir-Wingreen approach.[30–32] This remarkable physical effect will be described in detail in the following sections.

Coming to the conducting chain model, we find that the density and energy wavefronts, induced by the sudden change in temperature in the left reservoir, propa-
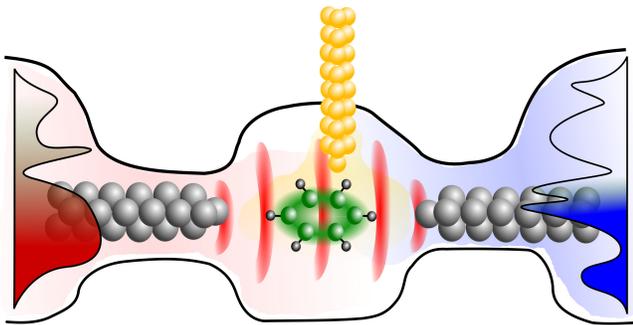
FIG. 1: (color online) Schematic transport setup where a nanoscale junction (central region) is connected to reservoirs via leads. When a temperature difference is applied to the leads by switching a thermo-mechanical potential a heat and charge current will flow through the device. The third lead (yellow) represents an additional "probe" lead, which can be used to determine the local temperature in the device. The spectral densities of the left and right reservoirs are also sketched, as they do, in principle, affect the transport.

gate with constant velocity, independent on the initial temperature or density. In contrast to this, at low temperatures we find characteristic Friedel oscillations in the steady-state distribution of the local temperature[10,12,33], a hallmark sign of quantum interference, with a periodicity depending on the Fermi wavelength, and, hence, the density.

In the present work we have not included the effect of electron-electron interaction. This can be taken into account within the framework of our recently proposed thermal Density-Functional Theory[22] with a suitable, e.g., local, approximation for the exchange-correlation potentials.

This paper is organized as follows: In Sec. II we introduce the model Hamiltonian employed to study the transient particle and energy density and their associated currents. In Sec. III we present a careful analysis of the transient behavior of a single-site impurity subject to a temperature gradient. Next, we discuss in Sec. IV the density and energy wave induced in a nanowire. Details of the numerical implementation are given in App. B. We conclude in Sec. V by summarizing our findings and providing an outlook on the implications for thermal Density-Functional Theory.

II. THERMOELECTRIC TRANSPORT IN NANOSCALE JUNCTIONS

A typical setup to study thermoelectric transport is shown in Fig. 1, where a molecular device or a nanowire is suspended between two metallic leads. If the device is exposed to a temperature gradient, e.g., by heating up the left lead, a heat or energy current and a charge current flow through the junction.

We model the aforementioned nano-junction by a

tight-binding Hamiltonian of the form

$$\hat{\mathcal{H}} = \sum_{\alpha k} \epsilon_{\alpha k} \hat{\phi}_{\alpha k}^{\dagger} \hat{\phi}_{\alpha k} + \sum_{mn} \hat{\phi}_n^{\dagger} H_{nm} \hat{\phi}_m$$
$$+ \sum_{\alpha k} \sum_m \left(\hat{\phi}_{\alpha k}^{\dagger} V_{(\alpha k)m} \hat{\phi}_m + \hat{\phi}_m^{\dagger} V_{m(\alpha k)} \hat{\phi}_{\alpha k} \right) \ . \quad (1)$$

where α labels leads connected to the central region. The electrons in the leads are governed by a dispersion $\epsilon_{\alpha k}$. We model the leads by an infinite tight-binding chain with nearest-neighbor hopping amplitudes t_α, which means that the dispersion reads explicitly

$$\epsilon_{\alpha k} = 2t_\alpha \cos(k) + \epsilon_\alpha \ . \quad (2)$$

It describes a single band with bandwidth $4t_\alpha$ and the positioning of the center of the band is determined by the lead-specific energy ϵ_α.

The central region is described by the generic Hamiltonian $\underline{\boldsymbol{H}}$, a matrix in the basis of the tight-binding sites which contains the kinetic energy, described by a uniform nearest-neighbor hopping t, and a local potential U_n, i.e.,

$$H_{mn} = t\delta_{m(n\pm 1)} + U_n \delta_{mn} \ , \quad (3)$$

The hopping amplitudes between leads and impurity are denoted by $\boldsymbol{V}_{\alpha k}$. Taking only a nearest-neighbor hopping between the last lead site and the closest site of the central region with amplitude $\boldsymbol{V}_\alpha$ we have

$$\boldsymbol{V}_{\alpha k} = \boldsymbol{V}_\alpha \sin(k) \ . \quad (4)$$

In the limit of infinite leads the sum over k corresponds to $\sum_k \equiv \frac{2}{\pi} \int_0^\pi \mathrm{d}k$. Hamiltonian (1) describes the intrinsic features of the system under consideration.

Usually, temperature-driven transport is described by removing the contacts between the central region and the leads in the initial preparation, and equilibrating the leads at different temperatures.[3,34] Then, at the initial time t_0, the device is suddenly contacted to the leads which induces a heat and charge transfer trough the central region. Here, by contrast, the initial state is determined for the fully contacted system. This is possible since we are employing Luttinger's thermo-mechanical potential to describe a gradient in the temperature. At t_0 we switch on a *thermal* and *charge* bias in the leads. This means that the Hamiltonian for $t > t_0$, which drives the system out of equilibrium is given by

$$\hat{\mathcal{H}}_{\text{drv}} = \sum_{\alpha k} \bar{\epsilon}_{\alpha k} \hat{\phi}_{\alpha k}^{\dagger} \hat{\phi}_{\alpha k} + \sum_{mn} \hat{\phi}_n^{\dagger} H_{nm} \hat{\phi}_m$$
$$+ \sum_{\alpha k} \sum_m \left(\hat{\phi}_{\alpha k}^{\dagger} V_{(\alpha k)m} \hat{\phi}_m + \hat{\phi}_m^{\dagger} V_{m(\alpha k)} \hat{\phi}_{\alpha k} \right) \ , \quad (5)$$

where the dispersion in the leads has changed to

$$\epsilon_{\alpha k} \to \bar{\epsilon}_{\alpha k} = (1 + \psi_\alpha)(\epsilon_{\alpha k} + U_\alpha) \ . \quad (6)$$

The potential bias U_α shifts the center of the band and the thermal bias ψ_α stretches the shifted bands. We have shown in a previous work,[26] that the application of the thermal bias ψ_α corresponds to changing the temperature in lead α by $\delta T_\alpha = \psi_\alpha T_0$, i.e., ψ_α determines the relative temperature change.
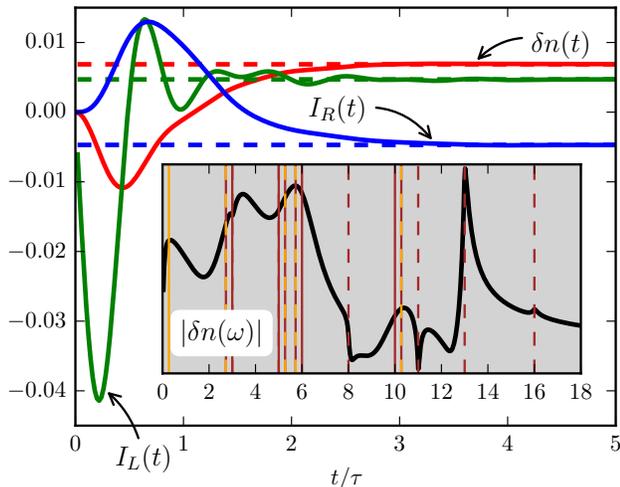
FIG. 2: (color online) Plot showing the transient density change, $\delta n(t)$, of the impurity site and the currents between left lead and impurity, $I_L(t)$, and right lead and impurity,$I_R(t)$, respectively. The corresponding steady-state value are indicated by the horizontal, dashed lines. The inset shows the Fourier transform of the density change of the long-time tail. The structure of this power spectrum reflects the distribution of energy levels in the leads.

III. TRANSIENT CURRENTS FOR A SINGLE-SITE IMPURITY

As a first example we consider a single-site impurity (quantum dot) coupled to two (symmetric) metallic leads. Specifically, we take the impurity site to be aligned with the chemical potential and the hopping amplitudes between the impurity and the leads are chosen as our unit of energy, i.e., $V_\alpha = V = 1$.(See also Appendix B for more details.)

The hopping amplitudes in both leads is $t_\alpha = 2V$, which means that the leads have a bandwidth of $8V$. Both leads are shifted down in energy by $-1V$ in order to break particle–hole symmetry, which is required to observe the Seebeck or Peltier effect, i.e., the interplay between charge and energy.[2] Accordingly, both the left and right lead have band edges which are positioned at $-5V$ (lower band edge) and $+3V$ (upper band edge) measured from the chemical potential, which is taken to define zero energy.

We stress that we do not take the wide-band limit. Accordingly, the embedding self-energy due to the leads does not only provide a finite lifetime for the impurity state, but also shifts its energy. For leads modeled by a tight-binding chain this shift is linear–as long as the impurity site lies within the band–and pushes the energy of the impurity above the chemical potential in the present scenario.

Initially the coupled system is equilibrated at a temperature $k_B T_0 = 0.25V$. Then, at $t = 0$, the temperature in the left lead is suddenly raised by applying a thermo-mechanical potential $\psi_L = 1$, which corresponds to a doubling of the temperature on the left side.

In Fig. 2 we show the transient change of the impurity density and the currents flowing to the left and right lead, respectively. A temperature-driven particle current occurs only because the system is not particle–hole symmetric. A perfect alignment of the center of both bands with the chemical potential and the impurity site would have two effects: 1) The energy of the impurity state would not be shifted, because the real part of the embedding self-energy vanishes at the center of the band. 2) The transmission would be symmetric, which implies that no net particle current flows.

The time scale τ in the plot of the transients in Fig. 2 represents the intrinsic time scale for the decay of electrons into the leads. The embedding self-energy due to lead α is proportional to V_α^2/t_α, which, in turn, implies a that the lifetime of the electrons due to the embedding is $\tau_\alpha \propto \hbar t_\alpha/2V_\alpha^2$. Since there are two leads we add the decay *rates* to get $\tau = \hbar t_\alpha/(2V^2) = \hbar/V$. For times $t > \tau$ the density (red line) and the currents from the left lead (green line) and the right lead (blue line) approach their respectively steady-state values (dashed lines). As expected, the current from the right lead is the negative of the current from the left lead in the steady-state regime. Furthermore the density change settles to a positive value which means that in the transient regime the impurity acquires additional particles. This can be expected since the impurity will increase its temperature due to the heating from the left lead. We recall that the energy of the impurity site is above the chemical potential, due to the coupling to the metallic leads, and hence a higher temperature results in an increase in density.
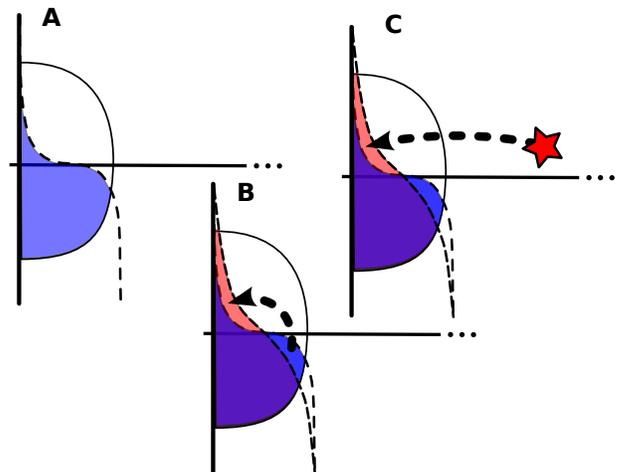

FIG. 3: (color online) Sketch showing the short time particle transfer processes: (A) The initial occupation of the left lead. (B) The sudden increase in temperature requires a redistribution of the electrons from below to above the chemical potential. (C) The presence of the impurity assist–at short times–this redistribution by providing electrons above the chemical potential and the impurity density drops initially.
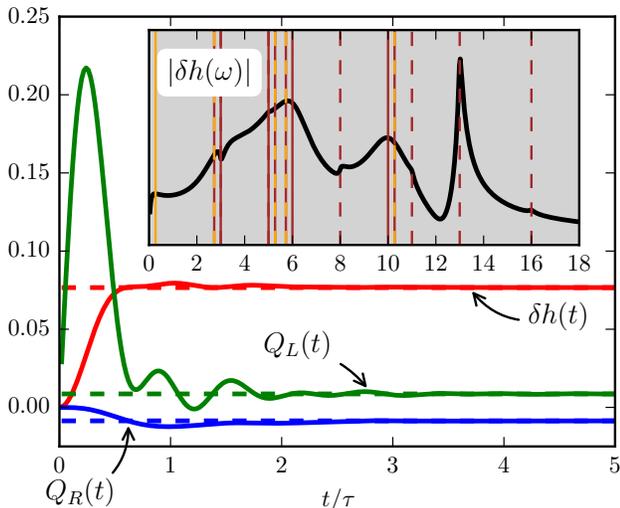
FIG. 4: (color online) Same as Fig. 2 but for the change in impurity energy, $\delta h(t)$, and left and right heat currents, $Q_L(t)$ and $Q_R(t)$, respectively.

Turning to the short-time transient, i.e., $t < \tau$, we see that the density of the impurity decreases, which seems to be counterintuitive. However we suggest a simple picture (cf. Fig. 3): The thermo-mechanical potential applied to the left lead forces the electrons to adjust to a higher temperature. This means that electrons have to be moved from below the chemical potential to above the chemical potential. The presence of the impurity site can facilitate this process, at least temporarily, by providing electrons above the chemical potential. This means that for short times electrons are "sucked" into the left lead, which decreases the impurity density. However, the impurity will have to take a higher temperature, and by extension density, itself. Now the right lead comes into play by providing electrons for the impurity.

This explanation is supported by the analysis of the transient currents. Initially there is a very strong flow from the impurity to the left lead ($t < 0.5\tau$). A little later we observe a flow from the right lead to the impurity $0.25\tau < t < \tau$. Finally, the two currents cross and settle at opposite steady-state values.

In Fig. 4 we show the time evolution of the impurity energy (red line) and its associated heat currents from the left lead (green line), and from the right lead (blue line). Since we heat up the system, it is always expected that the impurity energy increases, independent of the positioning of the impurity level. This is simply due to the fact that the energy is measured with respect to the chemical potential. Even if the impurity level would be below the chemical potential, which means that the state depopulates in the steady state, the change in energy would be positive, because we depopulate a *negative* energy state.

In light of the previous discussion of the particle flow at short times one may ask how it is possible to have a heat flow from the left lead to the impurity even though there are electrons moving above the chemical potential in the opposite direction. The resolution to this puzzle is the following: The energy of the impurity site is given by the impurity density times the local potential plus a contribution due to the hopping between the impurity and both leads.[43] In the present case the local potential is perfectly aligned with the chemical potential, i.e., the contribution from the local potential is zero. Accordingly, the only contribution to the local energy comes from the hopping to the leads. This (kinetic) energy does not depend on the "direction" of the hopping and therefore the local energy increases. Looking at the heat currents we see that there is initially a strong heat flow from the left lead to the impurity, followed by a much less pronounced heat flow from the impurity to the right lead. Finally, the flows equilibrate to the steady-state values.

The insets in both Figs. 2 and 4 show the Fourier transform of the density and energy change at long times. It is computed in a time window $t = [10\tau, 10\tau + \Delta t]$, where Δt is chosen big enough to resolve the "lowest" transition energy of our system, which in our example corresponds to transitions between the impurity level, ϵ_0, and the chemical potential ($\hbar\omega_{min} = \epsilon_0 \approx 0.27V$, vertical orange line). The sampling rate is taken to resolve the largest transition frequency, which is given by the energy differences of the thermally biased band edges of the left lead ($\hbar\omega_{max} = 16V$). In order to understand the possible transitions we recall that the band edges are initially at $-5V$ and $+3V$ for both the left and right lead. Applying the thermo-mechanical potential scales the left band by a factor of 2, which shifts the band edges of the left lead to $-10V$ and $+6V$, respectively. The solid, brown vertical lines depict transition frequencies from the band edges to the chemical potential, i.e., they are at $\hbar\omega = 3V, 5V, 6V, 10V$. Similarly, the dashed, brown vertical lines highlight transitions between band edges which correspond to $\hbar\omega = 3V, 5V, 8V, 11V, 13V, 16V$. Lastly, the dashed, brown–orange vertical lines indicate transitions between the band edges and the impurity level at $\hbar\omega = 3V - \epsilon_0, 5V + \epsilon_0, 6V - \epsilon_0, 10V + \epsilon_0$. Strong features of the Fourier spectrum coincide with the aforementioned transition frequencies. Note that in the wide band limit all features, except for the transition between the impurity level and the chemical potential at $\hbar\omega = \epsilon_0$, would be absent. The most distinct peak occurs for, both, the density and the energy at $\hbar\omega = 13V$, which refers to transitions between the lower band edge of the left lead and the upper band edge of the right lead.

IV. HEAT WAVE PROPAGATION THROUGH A CONDUCTING WIRE

Our second example describes a nanowire suspended between two metallic leads. The parameters for this system are taken to be identical to the single-impurity model discussed in the previous section. However, the
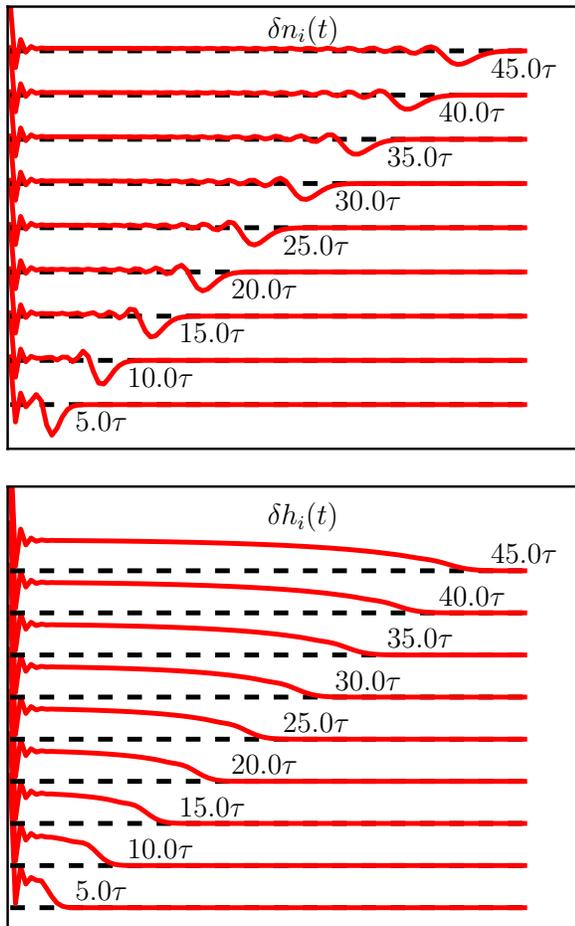
FIG. 5: (color online) Plot of the transient density and energy wave propagating through the nanowire. No external gate potential is applied. Both wavefronts propagate with the same velocity from the left to the right lead.
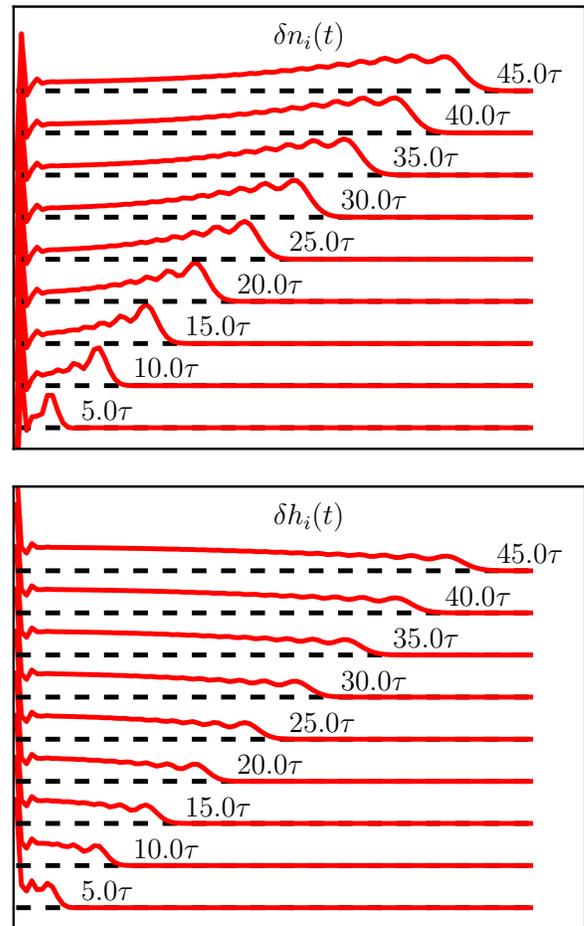
FIG. 6: (color online) Same as Fig. 5 but with an external gate potential. This reduces the initial density–and thereby the Fermi wave vector–of the nanowire. The transient wavefronts of the density and energy, however, propagate with the same velocity as with no external gate potential.

central region is composed of 100 sites connected by nearest neighbor hopping with amplitudes $t = V$. This means that the central region starts to form a band with bandwidth $4V$ and a dispersion given by the discretized version of Eq. (2). The center of the band representing the nanowire is aligned with the chemical potential.

In Fig. 5 we show snapshots of the spatially-resolved density and energy in the wire. The snapshots are taken at intervals of $\delta t = 5\tau$ up to the time $t < 50\tau$, just before the wavefronts reach the right end of the wire. First of all, we note that both the density and the energy wavefronts traverse the wire with the same constant velocity. This "Wiedemann-Franz"–like behavior can be understood from the fact that the energy is carried by the propagating electrons. Their spatial behavior, however, is different in the wake of the wavefront. As expected, the velocity of the wavefront is proportional to the hopping amplitude, i.e., $v \propto t$.

A slightly more refined guess for the velocity is the Fermi velocity, $v_{\rm F} \propto \partial_k \epsilon_k = 2t \sin(k_{\rm F})$. This implies a

density dependence of the velocity via the Fermi wave vector $k_{\rm F}$. In order to investigate whether there is a density dependence of the velocity we repeat the calculation with the dispersion of the nanowire shifted upwards by a constant gate potential $U_n = 1V$. In Fig. 6 we show snapshots of the density and energy changes for the gated nanowire. While the spatial form of the waves changes compared to the nanowire without any gate potential, the wavefront still moves with the same velocity. We do not find a density dependence.

Of course, the simplistic estimate of the velocity by the $v_{\rm F}$ has two caveats: 1) We inject a highly inhomogeneous wave packet in the nanowire, which implies that we have a superposition of many momentum states. Accordingly, it seems rather optimistic to assume that the wave packet is highly peaked around the Fermi wave vector. 2) The *initial* temperature is comparable to the bandwidth of the nanowire, i.e., $k_{\rm B}T_0 \lesssim 4t$. Hence, the thermal spread of occupations is of the order of the Fermi energy,
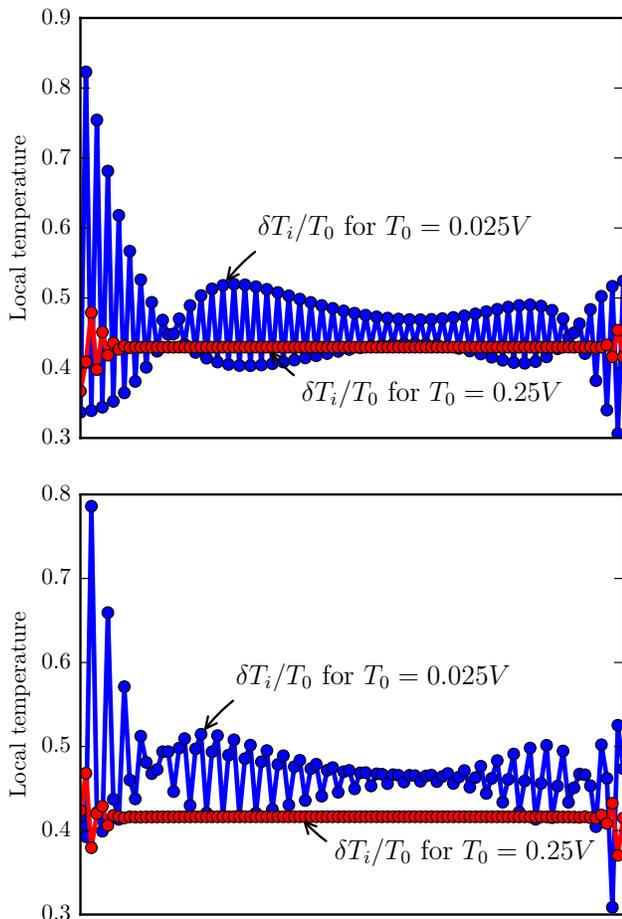
FIG. 7: (color online) Steady-state local temperature distributions in the nanowire determined by a "probe" lead as shown in Fig. 1. Both panels compare the local temperatures for different initial temperatures. The red lines correspond to an initial temperature of $k_B T_0 = 0.25V$ and the blue lines to $k_B T_0 = 0.025V$. The local temperature for the lower initial temperature exhibit typical $2k_F$ Friedel oscillations.

$\epsilon_F = -2V \cos(k_F) + 2V$. We have computed the transients of the density and energy with an initial temperature reduced by a factor of 10, i.e., $k_B T_0 = 0.025$. However, we find that– with and without the gate potential– the velocity of the wavefront corresponds to the velocity at the higher initial temperature. This leads to the conclusion that the spatial inhomogeneity of the wavefront requires a superposition of momentum states. We point out that it has recently been shown that the coordination of the tight-binding model affects the velocity of the wavefront.[35] It would be interesting to investigate if this geometric effect allows for different propagation velocities for density and energy waves.

Lastly, we look at the steady-state of the nanowire. We determine the local temperature and potential by introducing a third lead (cf. Fig. 1), which is weakly coupled to a specific site in the wire. Furthermore we take the wide-band limit for this additional lead. A local potential and temperature can be defined by imposing zero particle and energy current conditions for this "probe" lead.[29] It has been pointed out by us (cf. Ref. 26) that the zero current conditions are equivalent to asking: Which temperature and chemical potential reproduce the local density and energy under equilibrium conditions? It was also shown recently[36] that the local temperature obtained this way is comparable to that experimentally measurable in which one varies the temperature of the third lead till some observable of the system is minimally perturbed.[10]

In Fig. 7 we compare the local temperature computed for different initial temperatures. The upper panel depicts the local temperature for the wire without the gate. We can see that at low initial temperature ($k_B T_0 = 0.025V$, blue line) the local temperature oscillates from site to site, whereas for high initial temperature ($k_B T_0 = 0.25V$, red line) the spatial temperature profile is essentially flat. The lower panel shows temperature profiles for the gated nanowire. Qualitatively we see the same behavior as for the wire with no gate potential. However, the oscillations for low initial temperature now have a period of three lattice sites. The applied gate reduces the Fermi wave vector from $k_F = \pi/2a_0 \rightarrow k_F = \pi/3a_0$ (a_0 being the distance between neighboring sites). Accordingly, the oscillations in the local temperature correspond in both cases to "Friedel"–like oscillations at $q = 2k_F$. Friedel oscillations are a well-known feature of the degenerate electrons gas and represent a quantum interference effect. The average temperature variation of the wire is slightly below $\delta T/T_0 = 0.5$, i.e., the wire is closer in temperature to the colder right lead. We have already observed this phenomenon in Ref. 26, which was also predicted in Ref. 10,12. We conclude by mentioning that the local potential exhibits the same oscillations. The interested reader may find the corresponding plots in App. A.

V.   DISCUSSION AND CONCLUSION

In this paper we have investigated the transient currents induced by a temperature gradient. The temperature gradient has been applied by employing Luttinger's thermo-mechanical potential as proxy for temperature variations. Furthermore, the formulation in terms of the thermo-mechanical potential allowed us to study temperature-driven particle and energy transport in the so-called unpartitioned approach, where a nano scale device is already contacted to metallic leads in the initial preparation.

For a single-site impurity model we found that the transient particle current flows in the opposite direction to the steady-state current, which suggests that a frequency dependent generalization of the Seebeck coefficient changes sign at high frequencies. Furthermore, we provided a simple picture to interpret the numerical results for the transient particle current in terms of a impu-

rity assisted re–population of the electrons in the leads.

Considering a tight-binding chain, representing, e.g., conductive polymers or nanowires, we found that the velocity of the transient particle and energy wave is essentially constant over a range of initial temperatures and only depends on the hopping amplitudes. Furthermore we have shown that in the steady state there is a signature of quantum interference–at least at low temperatures. The local temperature and potential, as measured by a floating thermal probe exhibits characteristic $2k_\mathrm{F}$ Friedel oscillations.

Even though the model studied considered noninteracting particle, the results are highly relevant, since we have recently introduced a thermal Density-Functional Theory,[22] which allows to map the interacting system onto a fictitious non-interacting Kohn-Sham system.[37] In the future it will be interesting to investigate to what extent interactions, represented in terms of exchange-correlation corrections to the thermo-mechanical and charge potential will affect the presented results. We are confident that the presented results are an important step on the way to a fully microscopic description of the combined particle and energy transport in interacting systems.

Appendix A: Additional plots

In this appendix we provide additional plots. In Fig. 8 and 9 we show snapshots of the spatial profiles of the transient density and energy wave at low temperatures. In Fig. 10 we show the local potential determined from the steady-state density and energy of the nanowire.

Appendix B: Numerical details

The numerical computation of the time-dependent observables use two facts: 1) The system is noninteracting which allows for a direct solution of the equations of motion for the field operators. 2) The time evolution is triggered by a sudden change in the Hamiltonian. This means that we do not have to worry about time-ordering. The main complication comes due to the "openness" of the system, i.e., the coupling of a finite system to semi-infinite leads. It has be shown recently that if the leads are treated in the wide-band limit, the time-evolution can solved almost analytically.[38,39] In our calculation we do not take the wide-band limit and therefore we have to
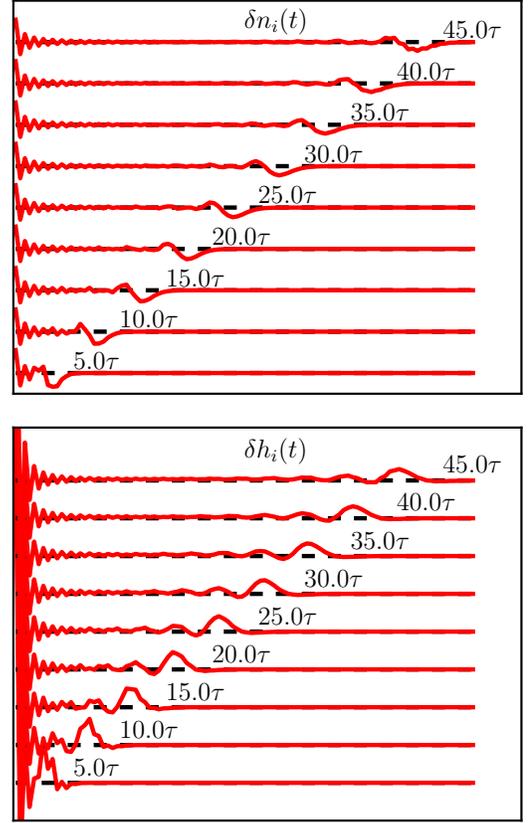

FIG. 8: (color online) Same as Fig. 5 in Sec. IV but with a reduced initial temperature $k_\mathrm{B}T_0 = 0.025V$. The velocity of the transient wavefront remains unaffected.

rely on a numerically solution of the involved integrals. In the following we provide a rough sketch of the numerical implementation, focusing on two key aspects: The evaluation of the Matsubara summation needed to represent the initial state, and the technique to compute the Fourier transform leading to the single-particle propagators. An introduction to nonequilibrium quantum systems may be found in Ref. 40.

Since the Hamiltonian (1), given in Sec. II, is noninteracting, we can formally solve for the time-dependent fields operators ($\hbar = 1$):

$$\hat{\boldsymbol{\phi}}\,(t) = \int_{-\infty}^{\infty} \frac{\mathrm{d}\omega}{2\pi i}\, e^{-i\omega t}\, \underline{\boldsymbol{G}}^\mathrm{R}(\omega)\cdot$$

$$\left(\hat{\boldsymbol{\phi}}\, + \sum_{\alpha k} \boldsymbol{V}_{\alpha k}^\star g_{\alpha k}^\mathrm{R}(\omega)\hat{\phi}_{\alpha k} \right)\,, \tag{B1a}$$

$$\hat{\phi}_{\alpha k}(t) = \int_{-\infty}^{\infty} \frac{\mathrm{d}\omega}{2\pi i}\, e^{-i\omega t} \left(g_{\alpha k}^\mathrm{R}(\omega)\hat{\phi}_{\alpha k} + g_{\alpha k}^\mathrm{R}(\omega)\boldsymbol{V}_{\alpha k}\cdot\underline{\boldsymbol{G}}^\mathrm{R}(\omega)\cdot \right.$$

$$\left. \left[\hat{\boldsymbol{\phi}}\, + \sum_{\alpha' k'} \boldsymbol{V}_{\alpha' k'}^\star g_{\alpha' k'}^\mathrm{R}(\omega)\hat{\phi}_{\alpha' k'} \right] \right)\,, \tag{B1b}$$

where $\hat{\boldsymbol{\phi}}$ denotes the vector of field operators referring
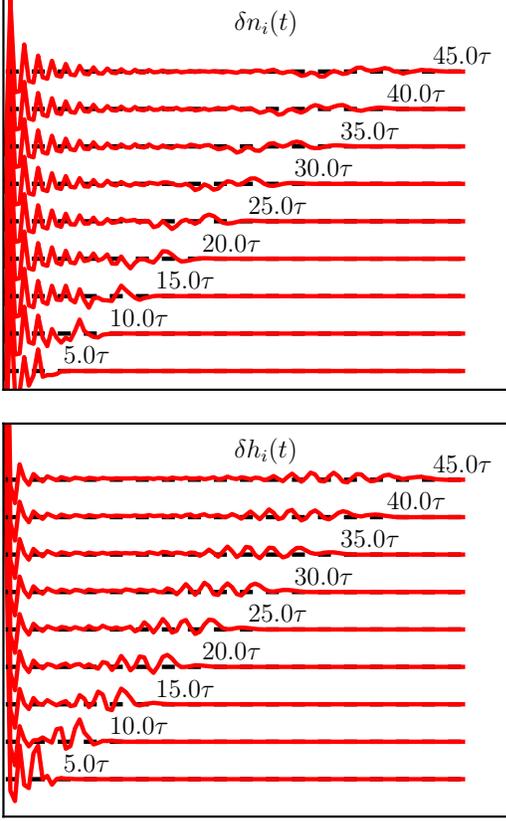
FIG. 9: (color online) Same as Fig. 6, Sec. IV but with initial temperature $k_{\mathrm{B}}T_0 = 0.025V$. Also for the case with an externally applied gate voltage the velocity of the wavefront is the same.
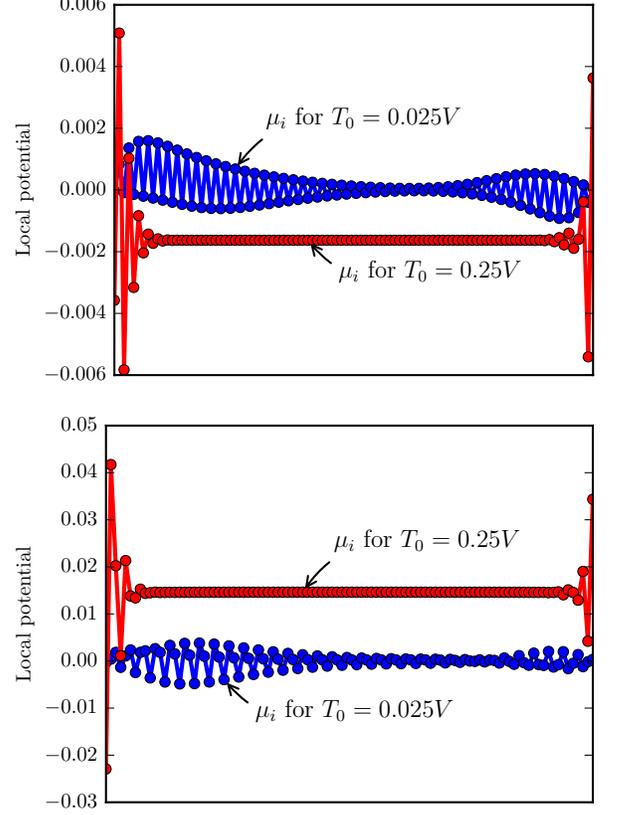

FIG. 10: (color online) Plots of the local potential of the nanowire studied in Sec. IV. The upper panel depicts the local potentials for the wire without an external gate and the lower panel with gate. Similar to the local temperature shown in Fig.7 the local potential exhibits Friedel oscillations with wave vector $q = 2k_{\mathrm{F}}$ for a low initial temperature.

to the central region. In Eq. (B1) we have introduced the device Green's function

$$\underline{G}(z) = \left(z - \underline{H} - \underline{\Sigma}(z)\right)^{-1} , \qquad (B2)$$

given in terms of the embedding self-energy,

$$\underline{\Sigma}(z) = \sum_{\alpha k} \boldsymbol{V}_{\alpha k}^{\star} g_{\alpha k}(z) \boldsymbol{V}_{\alpha k} , \qquad (B3)$$

and the Hamiltonian of the central region. $\underline{\Sigma}(z)$, in turn, is given in terms of the bare Green's functions of the leads,

$$g_{\alpha k}(z) = \left(z - \epsilon_{\alpha k}\right)^{-1} . \qquad (B4)$$

Using the explicit solution for the field operators we can write the time-dependent observables in terms of the initial state density matrices for the central region,

$$\left\langle \hat{\boldsymbol{\phi}}^{\dagger} \hat{\boldsymbol{\phi}} \right\rangle = \int_{-\infty}^{\infty} \frac{\mathrm{d}\epsilon}{2\pi i} \, f(\epsilon) \left[\underline{\boldsymbol{G}}^{\mathrm{A}}(\epsilon) - \underline{\boldsymbol{G}}^{\mathrm{R}}(\epsilon)\right] , \qquad (B5)$$

the boundary of the central region and the leads,

$$\left\langle \hat{\boldsymbol{\phi}}^{\dagger} \hat{\phi}_{\alpha k} \right\rangle = \int_{-\infty}^{\infty} \frac{\mathrm{d}\epsilon}{2\pi i} \, f(\epsilon) \left[g_{\alpha k}^{\mathrm{A}}(\epsilon) \boldsymbol{V}_{\alpha k} \cdot \underline{\boldsymbol{G}}^{\mathrm{A}}(\epsilon) \right. $$
$$\left. - g_{\alpha k}^{\mathrm{R}}(\epsilon) \boldsymbol{V}_{\alpha k} \cdot \underline{\boldsymbol{G}}^{\mathrm{R}}(\epsilon)\right] , \qquad (B6a)$$

$$\left\langle \hat{\phi}_{\alpha k}^{\dagger} \hat{\boldsymbol{\phi}} \right\rangle = \int_{-\infty}^{\infty} \frac{\mathrm{d}\epsilon}{2\pi i} \, f(\epsilon) \left[\underline{\boldsymbol{G}}^{\mathrm{A}}(\epsilon) \cdot \boldsymbol{V}_{\alpha k}^{\star} g_{\alpha k}^{\mathrm{A}}(\epsilon) \right. $$
$$\left. - \underline{\boldsymbol{G}}^{\mathrm{R}}(\epsilon) \cdot \boldsymbol{V}_{\alpha k}^{\star} g_{\alpha k}^{\mathrm{R}}(\epsilon)\right] , \qquad (B6b)$$

and the leads,

$$\left\langle \hat{\phi}_{\alpha' k'}^{\dagger} \hat{\phi}_{\alpha k} \right\rangle = \int_{-\infty}^{\infty} \frac{\mathrm{d}\epsilon}{2\pi i} \, f(\epsilon) \left(\delta_{\alpha \alpha'} \delta_{kk'} \left[g_{\alpha k}^{\mathrm{A}}(\epsilon) - g_{\alpha k}^{\mathrm{R}}(\epsilon)\right] \right. $$
$$+ \left[g_{\alpha k}^{\mathrm{A}}(\epsilon) \boldsymbol{V}_{\alpha k} \cdot \underline{\boldsymbol{G}}^{\mathrm{A}}(\epsilon) \cdot \boldsymbol{V}_{\alpha' k'}^{\star} g_{\alpha' k'}^{\mathrm{A}}(\epsilon) \quad (B7)$$
$$\left. - g_{\alpha k}^{\mathrm{R}}(\epsilon) \boldsymbol{V}_{\alpha k} \cdot \underline{\boldsymbol{G}}^{\mathrm{R}}(\epsilon) \cdot \boldsymbol{V}_{\alpha' k'}^{\star} g_{\alpha' k'}^{\mathrm{R}}(\epsilon)\right] \right) .$$

In order to numerically evaluate integrals of the form

$$\left\langle \hat{\phi}_\beta^\dagger \hat{\phi}_\alpha \right\rangle = \int_{-\infty}^{\infty} \frac{\mathrm{d}\epsilon}{2\pi i} \, f(\epsilon) \left[G_{\alpha\beta}^{\mathrm{A}}(\epsilon) - G_{\alpha\beta}^{\mathrm{R}}(\epsilon) \right] , \quad (\text{B8})$$

we use the following representation of the Fermi function:

$$f(z) = \frac{1}{2} - \sum_f \frac{R_f}{z - i z_f} . \quad (\text{B9})$$

The residues R_f and the *modified* Matsubara frequencies z_f can be obtained from the matrix

$$B_{j j+1} = B_{j+1 j} = \frac{1}{2\sqrt{(2j+1)(2j+3)}} , \quad 0 \le j . \quad (\text{B10})$$

Considering the eigenvalue problem

$$\underline{B} \cdot \boldsymbol{b}_f = b_f \boldsymbol{b} , \quad (\text{B11})$$

it can be shown[41] that z_f and R_f are given by

$$z_f = \frac{1}{\beta b_f} , \quad (\text{B12a})$$

$$R_f = \frac{1}{\beta} \left(\frac{\boldsymbol{b}_{f,0}}{2 b_f} \right)^2 , \quad (\text{B12b})$$

where $\boldsymbol{b}_{f,0}$ denotes the component $j = 0$ of the eigenvector. Now we can use Eq. (B9) in Eq. (B8) to obtain

$$\begin{aligned} \left\langle \hat{\phi}_\beta^\dagger \hat{\phi}_\alpha \right\rangle &= \sum_f R_f G_{\alpha\beta}^{\mathrm{M}}(i z_f) \\ &+ \frac{1}{2} \int_{-\infty}^{\infty} \frac{\mathrm{d}\epsilon}{2\pi i} \left[G_{\alpha\beta}^{\mathrm{A}}(\epsilon) - G_{\alpha\beta}^{\mathrm{R}}(\epsilon) \right] . \quad (\text{B13}) \end{aligned}$$

It has been shown that the truncated summation over z_f converges much faster than the original Matsubara summation.[42]

For the calculation of the propagators we have to perform Fourier integrals of the type

$$\int_{-\infty}^{\infty} \frac{\mathrm{d}\omega}{2\pi} \, e^{\mp i\omega t} F^{\mathrm{R/A}}(\omega) . \quad (\text{B14})$$

A straight-forward numerical evaluation is hampered by a strongly oscillating integrand for $t \gg \tau$, where τ is a characteristic time scale of the Hamiltonian. This can be avoided by closing the integration contour with an infinite semi-arc in the lower/upper half of the complex plane for $F^{\mathrm{R}}(\omega)/F^{\mathrm{A}}(\omega)$. However, the function $F^{\mathrm{R/A}}$ may has branch cuts on the real axis due to the embedding self-energy. Figure 11 shows how the branch cut can be rotated away from the real axis and directed along the negative (or positive) imaginary axis. The semi-arc has to be interrupted with integration contours running along the deformed branch cuts. We label these contours by $\mathcal{C}_\omega$. This allows us to write the Fourier transform as

$$\begin{aligned} \int_{-\infty}^{\infty} \frac{\mathrm{d}\omega}{2\pi} \, e^{\mp i\omega t} F^{\mathrm{R/A}}(\omega) &= -\left(\int_{\mathcal{C}_\omega} \frac{\mathrm{d}\omega}{2\pi} \, e^{\mp i\omega t} F^{\mathrm{R/A}}(\omega) \right. \\ &\left. \pm i \sum_m e^{\mp i\omega_m t} \mathrm{Res}\left[F^{\mathrm{R/A}}(\omega_m) \right] \right) , \quad (\text{B15}) \end{aligned}$$
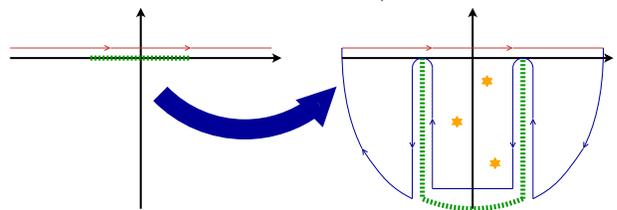

FIG. 11: (color online) Sketch showing how the original Fourier integration contour (red) for a retarded integrand is replaced by an interrupted semi circle (blue) in the lower half of the complex plane. However, in order to do so the branch cut (green dashes) needs to be rotated away from the real axis and oriented along the negative imaginary axis. In deforming the branch cut we analytically continue the retarded function into the lower half of the complex plane, which potentially "uncovers" poles (orange stars), e.g., poles representing the quasi-particle energy for the case of the Green's function. The contribution from the contour on the semi circle vanish due to the Fourier exponential. The remaining contour, running back and forth along the branch cut is denoted by $\mathcal{C}_\omega$ in Eq. (B15).

where ω_m are the poles in the lower/upper half of the complex plane of $F^{\mathrm{R/A}}(z)$, respectively. Since the contour $\mathcal{C}_\omega$ is always parallel to the imaginary axis, the Fourier exponentials are now exponentially decaying, which improves the numerical stability and allows us to compute the long-time behavior accurately and efficiently.

* eichf@missouri.edu
[1] G. S. Nolas, J. Sharp, and J. Goldsmid, *Thermoelectrics: Basic Principles and New Materials Developments* (Springer, New York, 2001).
[2] Y. Dubi and M. Di Ventra, Rev. Mod. Phys. **83**, 131 (2011), URL http://link.aps.org/doi/10.1103/RevModPhys.83.131.
[3] M. Di Ventra, *Electrical Transport in Nanoscale Systems* (Cambridge University Press, Cambridge, UK, 2008), URL http://dx.doi.org/10.1017/CBO9780511755606.
[4] A. Majumdar, Annual Review of Materials Science **29**, 505 (1999), http://dx.doi.org/10.1146/annurev.matsci.29.1.505, URL http://dx.doi.org/10.1146/annurev.matsci.29.1.505.
[5] Y.-J. Yu, M. Y. Han, S. Berciaud, A. B. Georgescu, T. F. Heinz, L. E. Brus, K. S. Kim, and P. Kim,

Applied Physics Letters **99**, 183105 (2011), URL http://scitation.aip.org/content/aip/journal/apl/99/18/10.1063/1.3657515.

[6] K. Kim, J. Chung, G. Hwang, O. Kwon, and J. S. Lee, ACS Nano **5**, 8700 (2011), http://pubs.acs.org/doi/pdf/10.1021/nn2026325, URL http://pubs.acs.org/doi/abs/10.1021/nn2026325.

[7] K. Kim, W. Jeong, W. Lee, and P. Reddy, ACS Nano **6**, 4248 (2012), http://pubs.acs.org/doi/pdf/10.1021/nn300774n, URL http://pubs.acs.org/doi/abs/10.1021/nn300774n.

[8] F. Menges, H. Riel, A. Stemmer, and B. Gotsmann, Nano Letters **12**, 596 (2012), http://pubs.acs.org/doi/pdf/10.1021/nl203169t, URL http://pubs.acs.org/doi/abs/10.1021/nl203169t.

[9] M. Mecklenburg, W. A. Hubbard, E. R. White, R. Dhall, S. B. Cronin, S. Aloni, and B. C. Regan, Science **347**, 629 (2015), http://www.sciencemag.org/content/347/6222/629.full.pdf, URL http://www.sciencemag.org/content/347/6222/629.abstract.

[10] Y. Dubi and M. Di Ventra, Nano Lett. **9**, 97 (2009), http://pubs.acs.org/doi/pdf/10.1021/nl8025407, URL http://pubs.acs.org/doi/abs/10.1021/nl8025407.

[11] D. Sánchez and R. López, Phys. Rev. Lett. **110**, 026804 (2013), URL http://link.aps.org/doi/10.1103/PhysRevLett.110.026804.

[12] J. P. Bergfield, M. A. Ratner, C. A. Stafford, and M. Di Ventra, Phys. Rev. B **91**, 125407 (2015), URL http://link.aps.org/doi/10.1103/PhysRevB.91.125407.

[13] J. P. Bergfield, S. M. Story, R. C. Stafford, and C. A. Stafford, ACS Nano **7**, 4429 (2013), http://pubs.acs.org/doi/pdf/10.1021/nn401027u, URL http://pubs.acs.org/doi/abs/10.1021/nn401027u.

[14] R. Biele, R. D'Agosta, and A. Rubio, Phys. Rev. Lett **115**, 056801 (2015), URL http://link.aps.org/doi/10.1103/PhysRevLett.115.056801.

[15] A. Shastry and C. A. Stafford, Phys. Rev. B **92**, 245417 (2015), URL http://link.aps.org/doi/10.1103/PhysRevB.92.245417.

[16] J. M. Luttinger, Phys. Rev. **135**, A1505 (1964), URL http://link.aps.org/doi/10.1103/PhysRev.135.A1505.

[17] B. S. Shastry, Rep. Prog. Phys. **72**, 016501 (2009), URL http://stacks.iop.org/0034-4885/72/i=1/a=016501.

[18] T. Qin, Q. Niu, and J. Shi, Phys. Rev. Lett. **107**, 236601 (2011), URL http://link.aps.org/doi/10.1103/PhysRevLett.107.236601.

[19] A. Shitade, Prog. Theor. Exp. Phys. **2014** (2014), URL http://ptep.oxfordjournals.org/content/2014/12/123I01.abstract.

[20] G. Tatara, Phys. Rev. Lett. **114**, 196601 (2015), URL http://link.aps.org/doi/10.1103/PhysRevLett.114.196601.

[21] G. Tatara, Phys. Rev. B **92**, 064405 (2015), URL http://link.aps.org/doi/10.1103/PhysRevB.92.064405.

[22] F. G. Eich, M. Di Ventra, and G. Vignale, Phys. Rev. Lett. **112**, 196401 (2014), URL http://link.aps.org/doi/10.1103/PhysRevLett.112.196401.

[23] R. Landauer, IBM J. Research and Development **1**, 223 (1957), ISSN 0018-8646.

[24] M. Büttiker, Y. Imry, R. Landauer, and S. Pinhas, Phys. Rev. B **31**, 6207 (1985), URL http://link.aps.org/doi/10.1103/PhysRevB.31.6207.

[25] R. Landauer, J. Phys.: Condens. Matter **1**, 8099 (1989), URL http://stacks.iop.org/0953-8984/1/i=43/a=011.

[26] F. G. Eich, A. Principi, M. Di Ventra, and G. Vignale, Phys. Rev. B **90**, 115116 (2014), URL http://link.aps.org/doi/10.1103/PhysRevB.90.115116.

[27] M. Cini, Phys. Rev. B **22**, 5887 (1980), URL http://link.aps.org/doi/10.1103/PhysRevB.22.5887.

[28] G. Stefanucci and C.-O. Almbladh, Phys. Rev. B **69**, 195318 (2004), URL http://link.aps.org/doi/10.1103/PhysRevB.69.195318.

[29] C. A. Stafford, ArXiv e-prints (2014), 1409.3179.

[30] Y. Meir and N. S. Wingreen, Phys. Rev. Lett. **68**, 2512 (1992), URL http://link.aps.org/doi/10.1103/PhysRevLett.68.2512.

[31] N. S. Wingreen, A.-P. Jauho, and Y. Meir, Phys. Rev. B **48**, 8487 (1993), URL http://link.aps.org/doi/10.1103/PhysRevB.48.8487.

[32] A.-P. Jauho, N. S. Wingreen, and Y. Meir, Phys. Rev. B **50**, 5528 (1994), URL http://link.aps.org/doi/10.1103/PhysRevB.50.5528.

[33] A. Caso, L. Arrachea, and G. S. Lozano, Phys. Rev. B **81**, 041301 (2010), URL http://link.aps.org/doi/10.1103/PhysRevB.81.041301.

[34] G. E. Topp, T. Brandes, and G. Schaller, EPL (Europhysics Letters) **110**, 67003 (2015), URL http://stacks.iop.org/0295-5075/110/i=6/a=67003.

[35] M. Metcalf, G.-W. Chern, M. Di Ventra, and C.-C. Chien, ArXiv e-prints (2015), 1502.04975.

[36] L. Ye, D. Hou, X. Zheng, Y. Yan, and M. Di Ventra, Phys. Rev. B **91**, 205106 (2015), URL http://link.aps.org/doi/10.1103/PhysRevB.91.205106.

[37] W. Kohn and L. J. Sham, Phys. Rev. **140**, A1133 (1965), URL http://link.aps.org/doi/10.1103/PhysRev.140.A1133.

[38] R. Tuovinen, R. van Leeuwen, E. Perfetto, and G. Stefanucci, Journal of Physics: Conference Series **427**, 012014 (2013), URL http://stacks.iop.org/1742-6596/427/i=1/a=012014.

[39] R. Tuovinen, E. Perfetto, G. Stefanucci, and R. van Leeuwen, Phys. Rev. B **89**, 085131 (2014), URL http://link.aps.org/doi/10.1103/PhysRevB.89.085131.

[40] G. Stefanucci and R. van Leeuwen, *Nonequilibrium Many-Body Theory of Quantum Systems: A Modern Introduction* (Cambridge University Press, Cambridge, 2013), ISBN 978-0-521-76617-3.

[41] T. Ozaki, Phys. Rev. B **75**, 035123 (2007), URL http://link.aps.org/doi/10.1103/PhysRevB.75.035123.

[42] C. Karrasch, V. Meden, and K. Schönhammer, Phys. Rev. B **82**, 125114 (2010), URL http://link.aps.org/doi/10.1103/PhysRevB.82.125114.

[43] We have adapted the convention to split the hopping energy equally between the participating sites.